CHEMISTRY OF MATERIALS

Article

pubs.acs.org/cm

Controlling the Thermoelectric Properties of Thiophene-Derived Single-Molecule Junctions

William B. Chang,[†,○] Cheng-Kang Mai,[‡,○] Michele Kotiuga,[§,∇,○] Jeffrey B. Neaton,[§,∇,⊥] Guillermo C. Bazan,[‡] and Rachel A. Segalman*[,†]

[†]Department of Chemical Engineering & Materials, University of California, Santa Barbara, California 93106, United States

[‡]Center for Polymers and Organic Solids, Departments of Chemistry & Biochemistry and Materials, University of California, Santa Barbara, California 93106, United States

[§]Department of Physics, University of California, Berkeley, California 94720, United States

[∇]Molecular Foundry, Lawrence Berkeley National Laboratory, Berkeley, California 94720, United States

[⊥]Kavli Energy NanoSciences Institute at Berkeley, Berkeley, California United States

Supporting Information

ABSTRACT: Thermoelectrics are famously challenging to optimize, because of inverse coupling of the Seebeck coefficient and electrical conductivity, both of which control the thermoelectric power factor. Inorganic−organic interfaces provide a promising route for realization of the strong electrical and thermal asymmetries required for thermoelectrics. In this work, transport properties of inorganic−organic interfaces are probed and understood at the molecular scale using the STM-break junction measurement technique, theory, and a class of newly synthesized molecules. We synthesized a series of disubstituted thiophene derivatives varying the length of alkylthio-linkers and the number of thiophene rings. These molecules allow the systematic tuning of electronic resonances within the junction. We observed that these molecules have a decreasing Seebeck coefficient with increasing length of the alkyl chain, while oligothiophene junctions show an increasing Seebeck coefficient with length. We find that thiophene−Au junctions have significantly higher Seebeck coefficients, compared to benzenedithiol (in the range of 7−15 μV/K). A minimal tight-binding model, including a gateway state associated with the S−Au bond, captures and explains both trends. This work identifies S−Au gateway states as being important and potentially tunable features of junction electronic structure for enhancing the power factor of organic/inorganic interfaces.

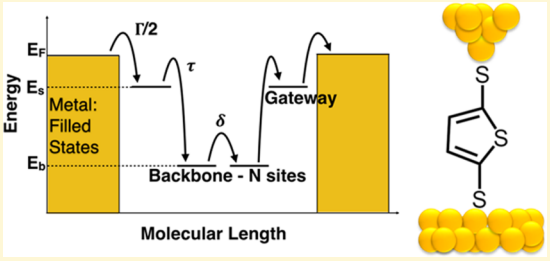

INTRODUCTION

In recent years, single molecule junctions have provided scientists with a unique manner to probe charge dynamics at the molecular scale and, in turn, understand how to tune the thermoelectric properties. A large interest lies in controlling and maximizing the power factor of molecular junctions: S^2G, where S is the Seebeck coefficient (also known as the thermopower) and G is the electrical conductance. S and G are inversely correlated in macroscopic materials, challenging researchers to maximize thermoelectric efficiencies by decoupling these two phenomena.

In junctions formed with small molecules strongly bonded to two electrodes, transport is typically dominated by tunneling: the so-called "Landauer transport regime".[1,2] In this coherent tunneling regime, the relative level alignment of the frontier orbital to the lead Fermi energy (E_F) and the nature of the bond, including the coupling of this level to the lead (Γ), dictate the magnitude and sign of G and S. Assuming the transmission function is an approximately Lorentzian function peaked at the frontier orbital resonance energy with broadening Γ, G increases with Γ, and as the resonance moves closer to E_F.[3] On the other hand, S is proportional to the negative logarithmic derivative of the transmission function, with respect to energy, evaluated at E_F, and increases as Γ decreases and the frontier orbital resonance moves closer to E_F.[4,5] Therefore, it is possible to couple S and G in new ways in a molecular junction with Lorentzian resonances, to maximize the power factor with junctions having a transmission function featuring a narrow frontier orbital resonance close to E_F. Experimentally, both S and G have been shown to increase simultaneously with energy level alignment.[3] Positioning the energy of the frontier highest occupied or lowest unoccupied molecular orbitals (HOMO or LUMO) closer to the E_F of gold will result in a simultaneous increase in both S and σ.[6,7,8−11] Other methods shown to control S^2G are by varying binding groups,[4,8,12−17] molecular design, and choice of metal contacts.[2,18−21]

In this work, the energetics of the junction were manipulated through modification of the molecular backbone while leaving the binding group constant. For this series of molecules, the thioacetate binding group was selected, because it binds strongly to gold. Because of the strength of the S−Au chemical bond,

Received: November 19, 2014

   dx.doi.org/10.1021/cm504254n | Chem. Mater. XXXX, XXX, XXX−XXX

there is a large charge localization at the metal/molecule interface, leading to a gateway state, which is an intermediary state coupling the lead to the molecular backbone. The effect of the gateway state under variation of the molecular backbone was examined. The electron transport through these junctions can be separated into two sequences: the transport into the molecule through the binding group, and transport within the molecule itself. It has been experimentally shown that the binding groups on each molecule dominate the coupling of the molecule to the electrode, resulting in varying peak breadths within the calculated transmission functions of these junctions.[22−24] The strength of the bond coupling the molecule to the gold electrodes determines the energetics of the metal/molecule interface, which has strong implications for S and G.

The concept that differences in molecular design can cause strong changes in the Seebeck coefficient of the molecular junction was examined. Evidently, the molecular design dictates the modes of electron transport within the channel. Thiophene-based molecular junctions, shown in Figure 1, were used to investigate this concept through two series: one consisted of thiophene molecules with increasing alkyl linker lengths (**TA** series: T1, TA2, and TA3) and the other had increased thiophene π-conjugated units (**OT** Series: T1, OT2 and OT3). Thiophene was chosen to study the effects of a higher HOMO energy, since thiophene has a HOMO energy closer to the E_F of gold than benzenedithiol.[25,26] By increasing the alkyl linker length in TA2 and TA3, the coupling of the molecular backbone and gateway state is expected to be reduced, leading to localization of charge on the thiophene core and a weaker peak in the transmission function gateway state. An increase in the conjugated backbone in OT2 and OT3 was designed to investigate the effects on conjugated molecular length coupling to a gateway state for a HOMO positioned very close to E_F. Detailed synthesis of all these molecules can be found in the Experimental Methods section. The experimental conductance and Seebeck coefficient measurement was performed in a custom-built STM-break junction setup, with experimental details provided in the method section below. Measurements of G for the molecular series T1, TA2, TA3 and T1, OT2, OT3 are presented which show a decreasing trend with length in both cases. S was measured for the same molecular series T1, TA2, TA3 and T1, OT2, OT3. The **OT** series showed a positive, increasing S with length and the **TA** series showed a positive S that decreases with length. A tight-binding model with a gateway state was employed to capture all of the experimentally observed trends reported herein.

EXPERIMENTAL RESULTS

The conductance of a single molecule junction as a function of length is viewed as a tunneling barrier between two electrodes, with an exponential decay parameter termed β, which differs based on the molecular backbone. To confirm that this holds true, the electrical conductance of molecules T1, TA2, TA3, OT2, and OT3, as shown in Figure 1, were investigated. The histograms of these conductance traces can be found in the SI. Experimental results for the conductance are presented, as a function of molecular length, and these results are compared to β-decay parameters of known conjugated and nonconjugated systems. The molecular length is defined to be from sulfur to sulfur between the two thiol terminations when the molecule is in a relaxed geometry (that is, as symmetric and straight as possible). The conductance of T1, TA2, TA3, OT2 and OT3

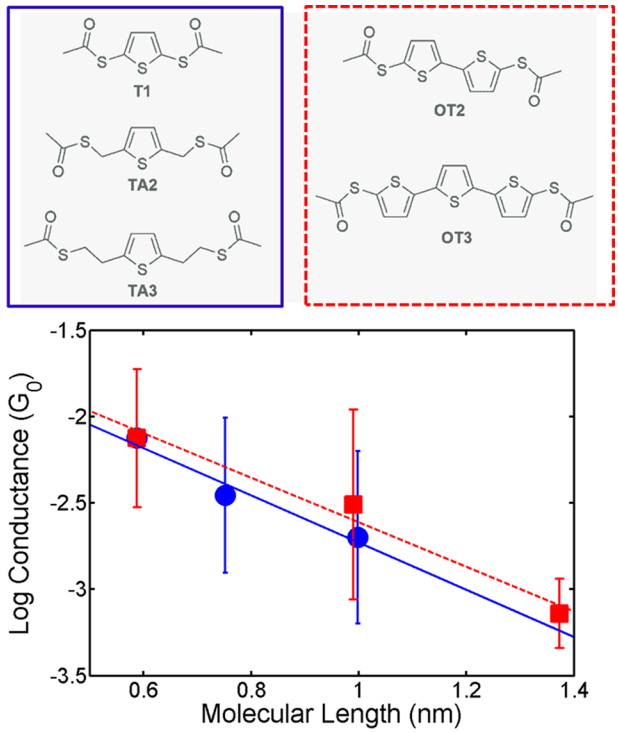

Figure 1. (Top) Chemical structures of molecules measured. The thioacetate binding group will be referred to as AcS (a) T1: (S,S′-thiophene-2,5-diyl diethanethioate), (b) TA2: (S,S′-thiophene-2,5-diylbis(methylene) diethanethioate), (c) TA3: (S,S′-2,2′-(thiophene-2,5-diyl)bis(ethane-2,1-diyl) diethanethioate (d) OT2: S,S′-([2,2′-bithiophene]-5,5′-diyl)diethanethioate (e) OT3: S,S′-([2,2:5′,2″-terthiophene]-5,5″-diyl) diethanethioate. (Bottom) Electrical conductance of molecular junctions with T1, TA2, and TA3 (blue circles) and T1, OT2 and OT3 (red squares) plotted as a function of molecular length. The data are fit to a standard exponential β-decay model. The β_{TA}-decay parameter is calculated to be 3.15 nm^{-1}, and the β_{OT}-decay parameter is calculated to be 2.96 nm^{-1}; these values show that increasing the alkyl linkers results in a β value that compares between the β value of π-conjugated systems and nonconjugated systems. The data points are the peak in the conductance histogram, and the error bars represent the full width at half-maximum of the histogram peaks, which can be found in the Suporting Information (SI), and do not represent instrumental error, but, instead, variances in binding geometry.

are $0.0075G_0$, $0.0035G_0$, $0.002G_0$, $0.0031G_0$, and $0.0007G_0$, respectively. These length-dependent values compare well to similar thiophene molecules in the literature.[25] This shows that T1 has a similar conductance, compared to more commonly studied molecules, such as benzenedithiol ($0.011G_0$) or benzenediamine (0.0064G0).[10] The experimental results indeed show an exponential decay in electrical conductance with molecular length, with T1, TA2, and TA3 having a β_{TA}-decay parameter of 3.15 nm^{-1} and T1, OT2, and OT3 having a β_{OT}-decay parameter of 2.96 nm^{-1}. Since it has been shown that a non-π-conjugated system has a β-decay parameter of 9.363 nm^{-1},[27] whiles a π-conjugated system has a β-decay parameter of 2.9 nm^{-1},[25] it can be inferred that additional non-π-conjugated linkers to a π-conjugated system results in behavior between that of a fully conjugated π-conjugated system and a non-conjugated system, because of partial delocalization of the electron over the molecule.

Additional information about the effects of π-conjugated versus nonconjugated molecular fragments on electron transmission can

dx.doi.org/10.1021/cm504254n | Chem. Mater. XXXX, XXX, XXX−XXX

be obtained from measurement of the Seebeck coefficient. Molecules in the TA series have an increasing number of alkyl linkers between the molecular ring and the binding group. This is intended to increase the spacing between the aromatic system and the electrodes, in order to isolate the molecule energy levels from the electrodes, which has been already seen to decrease the conductance more rapidly than the addition of conjugated units. The blue line in Figure 2 shows the Seebeck coefficient

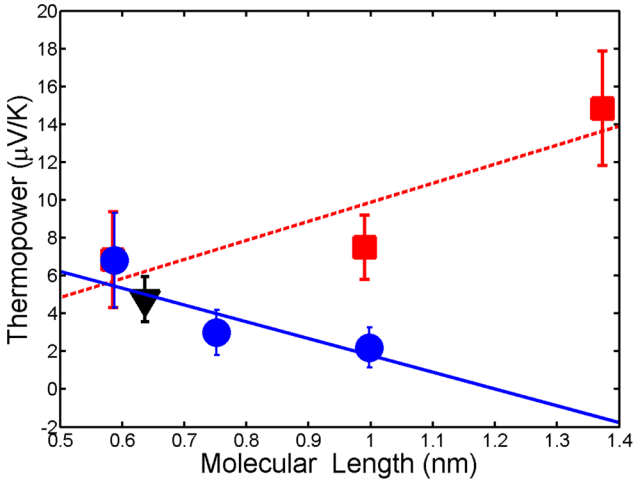

Figure 2. Seebeck coefficient of T1, TA2, TA3 (blue circle) and T1, OT2, OT3 (red square). T1 is in both **TA** and **OT**, and it is represented as a blue circle on a red square. Benzenedithiol was also measured in this setup (black triangle). The slope of the alkylthiophene (blue line) is −10.6 μV/(K nm) and corresponds well to literature trends on the Seebeck coefficient of pure alkanethiol junctions. The slope of the oligothiophene (red line) is 10.08 μV/(K nm), and is nearly double that of oligophenylthiols, the nearest comparable system.

measurements of the TA series, with respect to molecular length, and compares these values to benzenedithiol (black). The Seebeck coefficients for T1, TA2, and TA3 are 6.83, 3.01, and 2.2 μV/K, respectively. By fitting these numbers to a linear regression, the calculated slope is −10.6 μV/(K nm). In pure alkanethiol systems with no π-conjugation in the literature, the slope in the Seebeck coefficient is −5.6 μV/(K nm).[28] This demonstrates that the trend with the introduction of an alkyl linker to a π-conjugated system is not the same trend observed in solely nonconjugated or conjugated systems. As suggested with the length trend in conductance, the Seebeck coefficient decrease is larger than with pure alkane systems, and may be due to electron delocalization across the molecule, resulting in a system between that of a purely alkyl non-π-conjugated system and a fully π-conjugated system.[28]

In comparison, the Seebeck coefficients of oligothiophenes were also measured, where the increase in molecular length was due to additional π-conjugated systems, and not alkyl spacer groups. The red trend in Figure 2 shows that the Seebeck coefficients of T1, OT2 and OT3, which have an increase in conjugated molecular length, compared to molecules in the blue trend, which have increases in nonconjugated molecular length. By increasing the molecular π-conjugation length, an increase in the Seebeck coefficient was observed. The Seebeck coefficients of T1, OT2, and OT3 are 6.83, 7.49, and 14.84 μV/K, respectively, with a calculated slope of the Seebeck coefficient, with respect to molecular length of 10.08 μV/(K nm). Oligophenyls with amine and thiol binding groups, which is a similar system studied in the literature, also demonstrate an increase in Seebeck coefficient with increasing molecular length. The slope of the Seebeck coefficient, with respect to molecular length, for oligophenyldithiols is 6.9 μV/(K nm).[28] The larger Seebeck coefficient measured for T1 (6.83 μV/K), compared to benzenedithiol on this system (4.8 μV/K), shows the effect that using heterocycles with better HOMO energy alignment to the gold E_F increases S without lowering G.

THEORETICAL MODEL

To quantitatively model transport properties of a junction, there are two key ingredients: an accurate representation of how the molecule binds to the leads (junction geometry more generally), and a quantitative description of the level alignment of the molecular orbital resonance energies, with respect to the lead Fermi energy (E_F).[4] For thiol-terminated molecules, broad conductance histograms are measured compared to other terminal binding groups,[29] resulting from the sensitivity of conductance, with respect to binding geometry, which is highly variable, because of the nondirectionality of the S−Au bond,[30] posing challenges to theory in developing representative junction geometries. In addition, even if suitable model geometries existed, first-principles density functional theory (DFT) approaches are widely known to lead to incorrect level alignment,[31,32] resulting in an artificially low tunnel barrier and an overestimation of the conductance by an order of magnitude or more.[33] While GW-based self-energy corrections can improve the description of level alignment in the junction, corrections come at considerable computational expense, even for well-defined geometries.

We use a physically motivated tight-binding model with a minimal number of parameters, following previous work on strongly bound molecules;[25,34] our model is sufficient to explain measured trends in junction G and S, and provides a basis for interpreting future *ab initio* calculations. In our tight binding model, the leads are coupled via a broadening Γ to a gateway state, at energy E_s, localized on the thiol; this gateway state is, in turn, coupled to the molecular backbone at energy E_b with off-diagonal coupling strength τ. For molecules with N thiophene rings, we introduce N sites along the backbone with inter-ring hopping parametrized by δ. Using these parameters, the Hamiltonian ($\mathcal{H}$), for OT2 can be expressed as

$$\mathcal{H} = \begin{pmatrix} E_s - i\left(\frac{\Gamma}{2}\right) & \tau & 0 & 0 \\ \tau & E_b & \delta & 0 \\ 0 & \delta & E_b & \tau \\ 0 & 0 & \tau & E_s - i\left(\frac{\Gamma}{2}\right) \end{pmatrix}$$

As noted in previous works on related systems,[25] the gateway state arises from the strong S−Au bond formed in the absence of the hydrogen, allowing for strong hybridization and large charge localization. For example, gateway states can be seen in the transmission calculations of alkanedithiols of increasing length in the work of Li et al.[35] It can be shown that the positive and decreasing S, as a function of length, for the alkylthiophene molecular series T1, TA2, TA3 is a direct consequence of this gateway state. Initially the parameters in the model were fit to the measurements of the oligothiophenedithiol−Au junction (T1, OT2, OT3) G and S; the model was then extended to

dx.doi.org/10.1021/cm504254n | *Chem. Mater.* XXXX, XXX, XXX−XXX

incorporate the addition of CH_2 groups in order to the capture the behavior observed from TA2 and TA3.

To model the **OT** series, the data were fit to the model varying the parameters Γ, E_s, E_b, δ, and τ, and the experimental trends are replicated. As shown in Figure 3, the Seebeck

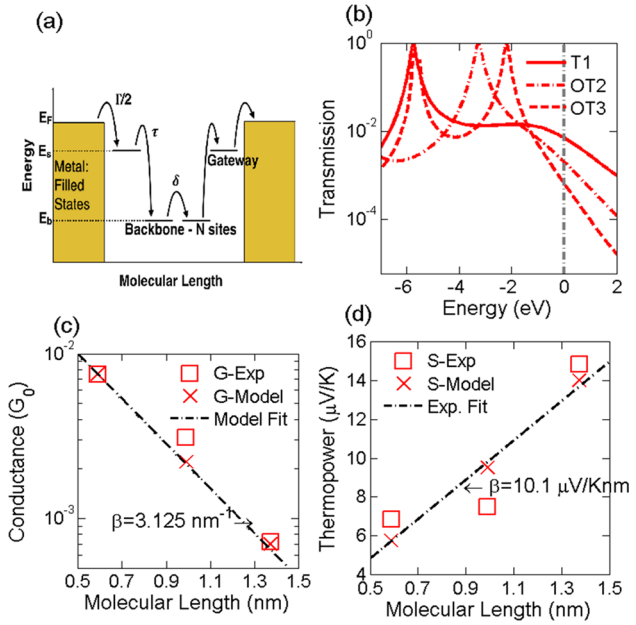

Figure 3. (a) Schematic of tight-binding model being used with multiple sites along the molecular backbone. (b) The calculated transmission values for the set of parameters: Γ = 5.32 eV, E_s = −0.98 eV, E_b = −5.54 eV, δ = −2.40 eV, and τ = −0.83 eV. (c) The corresponding conductance values, as predicted by the model. (d) Calculated Seebeck coefficient values, compared to experiment.

coefficient increases with length and the conductance decreases with exponentially length, with a decay constant ranging from 3−5 nm^{-1}, comparable to reported values for other conjugated backbones. The T1 transmission function, shown in red in Figure 3b, resulting from the best-fit parameters, clearly indicates features associated with the gateway state just below E_F.

For the molecules TA2 and TA3, the T1 Hamiltonian is extended to incorporate more sites representing additional CH_2 groups by allowing the position of the gateway state (E_s), to move up in energy toward E_F and the value of τ to decrease. The changes in these two parameters physically represent a decrease in overlap between the charge density on the thiol and the thiophene frontier states. Under this decoupling along the molecule, represented by the decrease in τ, the gateway state can interact more strongly with the gold, resulting in a shifted gateway state energy. Using the Γ and E_b values from the **OT** series, the model is fit via $E_{s,TA2}$, $E_{s,TA3}$, τ_{TA2}, and τ_{TA3}. In the model, it is observed that the decrease in τ contributes primarily to the decrease in the conductance as a function of length, where the shift in energy of the gateway state is the crucial element to capture the decrease in Seebeck coefficient, as a function of molecular length. The conductance and Seebeck coefficient values from the model are compared to experiment in Figure 4b and the transmission curves in Figure 4a, which again clearly show the resonance due to the gateway state just below E_F, whereas the HOMO resonance is a few electron volts below E_F. If a different starting point from the **OT** series is used, the same trends are produced with similar error bars.

Other efforts to capture this behavior for reduced tight-binding models without gateway states fail. With a single level alone, the only way to achieve a decreasing G and S with length is to move the frontier orbital away from E_F by a very large unphysical energy shift. If we introduce a second level, a set of parameters for which S is positive and decreasing with length can be found; however, the conductance increases with length, which is another unphysical result. Only this tight binding model with a gateway state is able to re-create the trends observed in experiment.

CONCLUSION

Thiophene junctions have a higher Seebeck coefficient and conductance, because of closer alignment of the highest occupied molecular orbital (HOMO) energy with the gold Fermi energy (E_F). By incorporating alkane linkers of increasing length between the binding group and thiophene, the molecular orbitals are localized, resulting in both a decreasing conductance and Seebeck coefficient. In oligothiophene junctions with increased conjugated units, an increase in the Seebeck coefficient was observed. This increase in Seebeck coefficient is attributed to a shift in the HOMO energy closer to the Fermi energy of gold, along with a sharpening of this peak in the transmission function. This highlights the needs for design rules, as an increase in molecular length will result in a decrease of conductance, but may increase or decrease the Seebeck coefficient, depending on the molecular design and the presence of a gateway state.

EXPERIMENTAL METHODS

Synthesis. All glassware was oven-dried or flame-dried, and the reactions were conducted under an argon atmosphere, using the

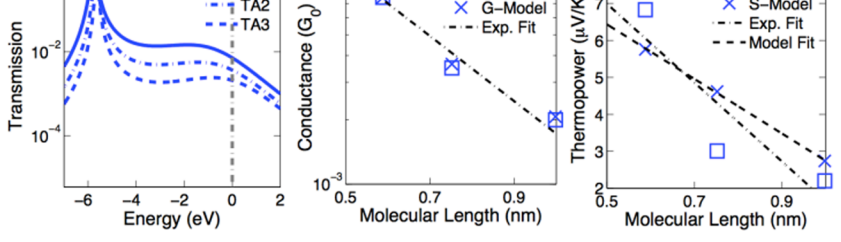

Figure 4. (a) Transmission curves for T1, TA2, TA3 with the parameters: Γ = 5.32 eV, E_b = −5.54 eV, and E_s = −0.98, −0.59. −0.10 eV, τ = −0.83, −0.68, −0.58 eV for T1, TA2, TA3 respectively. (b) Conductance predicted by the model and compared to experiment. (c) The Seebeck coefficient from the model, compared to the experimental values.

dx.doi.org/10.1021/cm504254n | Chem. Mater. XXXX, XXX, XXX−XXX

schlenk line technique. THF, DMF and diethyl ether were obtained via a solvent purification system packed with alumina. Unless specifically mentioned, all chemicals are commercially available and were used as received. Flash chromatography was performed using 60 Å silica gel (37−75 μm). ^{1}H NMR spectra were recorded at either 500 or 600 MHz, and ^{13}C NMR spectra were recorded at 100 or 126 MHz in $CDCl_3$. Chemical shifts are reported in units of ppm, referenced to residual solvent peak as follows: 7.24 ppm for ^{1}H NMR; 77.16 ppm for ^{13}C NMR.

S,S′-Thiophene-2,5-diyl Diethanethioate (T1).

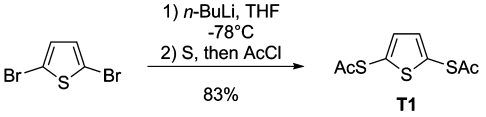

2,5-Dibromothiophene (1.98 g, 8.18 mmol, 1.0 equiv) was dissolved in dry Et_2O (40 mL), and the solution was cooled to −78 °C. *n*-BuLi (2.5 M in hexanes, 7.20 mL, 18.0 mmol, 2.2 equiv) was added dropwise via syringe, and the reaction was allowed to stir at −78 °C for 30 min. Dry sulfur (786 mg, 24.5 mmol, 3.0 equiv) powder was added in one portion, and the reaction was stirred for another hour before AcCl (1.45 mL, 20.4 mmol, 2.5 equiv) was added via syringe. The cold bath was removed, and the reaction was stirred for an additional 1 h, before pouring into water (50 mL). The aqueous layer was extracted with Et_2O (30 mL × 2), and the combined organic layers were washed with brine (10 mL), dried over $MgSO_4$, filtered, and concentrated to provide a gray oil. Purification by flash chromatography with a gradient of 1:1 hexane:CH_2Cl_2 to CH_2Cl_2 provided **T1** as a colorless oil (1.58 g, 83%). ^{1}H NMR (500 MHz, $CDCl_3$): δ 7.10 (s, 2H), 2.39 (s, 6H). ^{13}C NMR (126 MHz, $CDCl_3$): δ 193.00, 135.42, 131.17, 29.73. GC-MS: m/z = 232.

S,S′-Thiophene-2,5-diylbis(methylene) Diethanethioate (TA2).

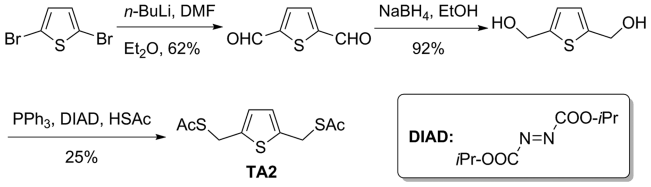

2,5-Dibromothiophene was converted to 2,5-diformylthiophene via lithium-halogen exchange, followed by trapping with DMF[36] and, subsequently, to thiophene-2,5-diyldimethanol via reduction with $NaBH_4$ following the known procedures.[37] TA2 was obtained via Mitsunobu reaction shown as follows.

Diisopropyl azodicarboxylate (DIAD, 1.06 mL, 3.38 mmol, 1.0 equiv) was added dropwise via a syringe into a dry THF (10 mL) solution of PPh_3 (1.41 g, 5.38 mmol, 2.5 equiv) in an ice bath. Thiophene-2,5-diyldimethanol (310 mg, 2.15 mmol, 1.0 equiv) was dissolved in dry THF (12 mL), and added slowly via a syringe to the above solution, followed by the addition of AcSH (380 μL, 5.38 mmol, 2.5 equiv). The reaction was allowed to warm to room temperature slowly and stir overnight (24 h), and then heated to 70 °C for 2 h. After cooling to room temperature, the reaction mixture was concentrated, and purified by flash chromatography (1:1 hexane:CH_2Cl_2) to provide TA2 as a colorless oil (141 mg, 25%). ^{1}H NMR (500 MHz, $CDCl_3$): δ 6.72 (s, 2H), 4.21 (s, 4H), 2.32 (s, 6H). ^{13}C NMR (126 MHz, $CDCl_3$): δ 194.72, 140.09, 126.47, 30.43, 28.28. GC-MS: m/z = 260.

S,S′-Thiophene-2,5-diylbis(methylene) Diethanethioate (TA3).

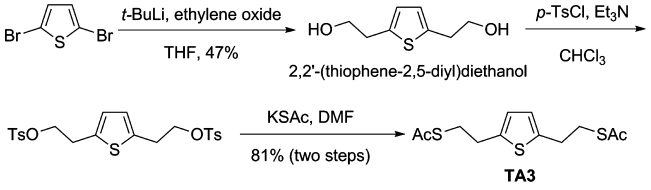

2,5-Dibromothiophene (1.84 g, 7.61 mmol, 1.0 equiv) was dissolved in dry THF (38 mL), and the solution was cooled to −78 °C in a dry ice/acetone bath. *t*-BuLi (9.84 mL of 1.7 M in pentane, 16.7 mmol, 2.2 equiv) was added dropwise via a syringe. The reaction was stirred at −78 °C for 30 min, and at 0 °C for 1 h, before cold ethylene peroxide (1.9 mL, 38.0 mmol, 5.0 equiv) was added quickly via a syringe. The reaction was allowed to warm to room temperature and was stirred overnight (15 h) and quenched with saturated NH_4Cl (aq, 20 mL). The aqueous layer was extracted with $CHCl_3$ (20 mL × 3). The combined organic layers were dried ($MgSO_4$), filtered, and concentrated to provide a brown oil. Purification by flash chromatography (1:1 hexane:EtOAc) provides 2,2′-(thiophene-2,5-diyl)diethanol as a colorless oil (616 mg, 47%). ^{1}H NMR (500 MHz, $CDCl_3$) δ 6.65 (s, 2H), 3.75 (t, J = 6.3 Hz, 4H), 2.94 (t, J = 6.3 Hz, 4H), 2.47 (s, 2H). ^{13}C NMR (126 MHz, $CDCl_3$): δ 139.62, 125.44, 63.38, 33.52. GC-MS: m/z = 172.

2,2′-(Thiophene-2,5-diyl)diethanol (198 mg, 1.15 mmol, 1.0 equiv) was dissolved in $CHCl_3$ (5 mL), Et_3N (480 μL, 3.45 mmol, 3.0 equiv), *p*-TsCl (482 mg, 2.53 mmol, 2.1 equiv) in $CHCl_3$ (3 mL), and catalytic amount of DMAP (5%) were added. After stirring at room temperature overnight (24 h), the reaction was diluted with H_2O (20 mL), and the aqueous layer was extracted with $CHCl_3$ (20 mL × 2). The combined organic layers were dried ($MgSO_4$), filtered, and concentrated to provide 2,2′-(thiophene-2,5-diyl)bis-(ethane-2,1-diyl)bis(4-methylbenzenesulfonate) as a brown oil, which was used without further purification. The analytical sample as a colorless oil was purified by flash chromatography (3:1 hexanes:EtOAc). ^{1}H NMR (600 MHz, $CDCl_3$): δ 7.72 (d, J = 8.1 Hz, 4H), 7.30 (d, J = 8.1 Hz, 4H), 6.56 (s, 2H), 4.14 (t, J = 6.8 Hz, 4H), 3.04 (t, J = 6.8 Hz, 4H), 2.42 (s, 6H). ^{13}C NMR (151 MHz, $CDCl_3$): δ 144.99, 137.25, 132.92, 129.96, 127.96, 126.05, 70.04, 29.78, 21.74. MS (ESI) m/z calcd for $C_{22}H_{24}O_6S_3Na^+$: 503.1; found: 503.1.

The crude product and KSAc (657 mg, 5.75 mmol, 5.0 equiv) were combined in a 25-mL round-bottom flask, dry DMF (12 mL) was added, and the suspension was stirred at 80 °C for 3 h. The reaction was diluted with H_2O (50 mL) and Et_2O (50 mL), and the aqueous layer was extracted with Et_2O (50 mL × 2). The combined organic layers were washed with H_2O (30 mL × 4), brine (20 mL), dried ($MgSO_4$), filtered, and concentrated to provide a yellow crystalline solid. Purification by flash chromatography (1:1 hexanes:$CHCl_3$, then $CHCl_3$) provided TA3 as a colorless crystalline solid (268 mg, 81% over two steps). ^{1}H NMR (500 MHz, $CDCl_3$): δ 6.61 (s, 2H), 3.08 (t, J = 7.4 Hz, 4H), 2.97 (t, J = 7.1 Hz, 4H), 2.29 (s, 6H). ^{13}C NMR (126 MHz, $CDCl_3$): δ 195.37, 140.93, 124.87, 30.66, 30.64, 30.21. MS (EI): m/z = 288.03.

S,S′-([2,2′-bithiophene]-5,5′-diyl) Diethanethioate (OT2).

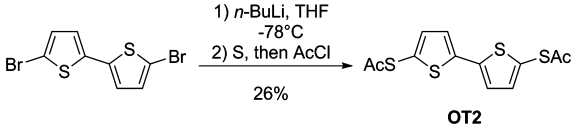

2,5-Dibromothiophene (405 mg, 1.25 mmol, 1.0 equiv) was dissolved in dry THF (25 mL), and the solution was cooled to −78 °C. *n*-BuLi (2.5 M in hexanes, 1.25 mL, 3.125 mmol, 2.5 equiv) was added dropwise via a syringe, and the reaction was allowed to stir at −78 °C for 30 min, and 0 °C for 1 h. Dry sulfur (120 mg, 3.75 mmol, 3.0 equiv) powder was added in one portion, and the reaction was stirred at 0 °C for another hour, before AcCl (267 μL, 3.75 mmol, 3.0 equiv) was added via a syringe. The reaction was allowed to warm to RT and stirred overnight (15 h), before pouring into water (50 mL). The aqueous layer was extracted with Et_2O (30 mL × 2), and the combined organic layers were washed with brine (10 mL), dried over $MgSO_4$, filtered, and concentrated to provide a brown oil. Purification by flash chromatography with a gradient of 1:1 hexane:$CHCl_3$ to $CHCl_3$ provided OT2 as a yellowish solid (102 mg, 26%). ^{1}H NMR (500 MHz, $CDCl_3$): δ 7.14 (d, J = 3.8 Hz, 2H), 7.04 (d, J = 3.8 Hz, 2H), 2.41 (s, 6H). ^{13}C NMR (126 MHz, $CDCl_3$): δ 194.00, 142.72, 136.66, 125.13, 125.05, 29.83.

S,S′-([2,2:5′,2″-terthiophene]-5,5″-diyl) Diethanethioate (OT3).

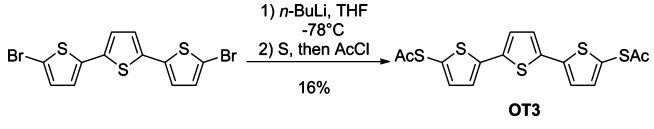

dx.doi.org/10.1021/cm504254n | Chem. Mater. XXXX, XXX, XXX−XXX

OT3 was synthesized under similar conditions as OT2,[38] and purified by flash chromatography with 3:2 hexane:CH_2Cl_2 to provide a yellowish solid (yield = 16%). ^{1}H NMR (600 MHz, $CDCl_3$) δ 7.12 (d, J = 3.7 Hz, 2H), 7.06 (s, 2H), 7.04 (d, J = 3.8 Hz, 2H), 2.41 (s, 6H). ^{13}C NMR (151 MHz, $CDCl_3$): δ 194.10, 143.10, 136.70, 136.26, 125.34, 124.42, 124.37, 29.75.

Measurement. Five microliters (5 μL) of a 0.05 M THF solution with the desired molecule at concentration of 10 mg/mL was drop-cast by micropipette onto gold films. The gold films were thermally evaporated onto a freshly cleaved mica substrate to enable an atomically smooth surface. A modified STM-break junction with a gold tip is then crashed into the gold substrate and withdrawn, with current and voltage measurements being acquired throughout the process. Both the STM Au tips and the Au thin films on mica were hydrogen-flame-annealed to ensure the removal of containments.

The measurement of the molecular conductance requires a bias of 5 mV to be applied between tip and substrate upon approach. The STM gold tip is driven to the gold substrate with a rate of 1 nm/s until a conductance threshold of $1G_0$ is reached. The tip is then withdrawn at a rate of 0.5 nm/s, with an Au−Au junction first forming, followed by a junction with the molecule of interest. No voltage bias is applied upon the withdrawal process. This process is repeated until 5000 junction traces are acquired. These results are then analyzed by histogram statistics and the resulting histogram peaks gives the molecular conductance, with the full width at half maximum (fwhm) of the peak being the error bar.

The measurement of the Seebeck coefficient (S) required a temperature gradient across the substrate and tip. The substrate was heated via a specially constructed STM cell and Peltier heater, and the STM tip was connected to a thermal sink to ensure a constant temperature of 20 °C. The power output to the Peltier heater was varied to control the temperature of the substrate. The gold STM tip is driven into the gold substrate until a conductance of $5G_0$ is measured. The tip−substrate voltage bias is then removed via a solid-state relay, and this cycle is repeated until 2000 junctions are acquired. Each trace is binned into a histogram. The peak voltage is the thermoelectric voltage at that temperature, and the fwhm is the error bar. S is calculated via a least-squares linear fit of the measured molecule, with the temperature drop as the independent variable, the peak voltage as the dependent variable, and the fwhm approximating the error in the measurement. Per convention, S is the negative of the resulting slope. A subtraction of the Seebeck coefficient of the instrument (1.6 μV/K) is then performed.

Theory. To calculate the conductance and Seebeck coefficient from the Hamiltonian $\mathcal{H}$, the Green's function (G) is constructed,

$$G^r = (\varepsilon - \mathcal{H})^{-1}$$

which, along with the coupling, is used to calculate the transmission via the standard expression

$$T = \mathrm{Tr}[\Gamma G^r \Gamma G^a]$$

where G^r is the retarded Green's function and G^a is the advanced Green's function. The transmission is related to the conductance and thermopower through the following relations:

$$G = G_0 T(E_F)$$

$$S = -\frac{\pi^2 k_B{}^2 T}{3e^2}\frac{\mathrm{d}}{\mathrm{d}E}\ln T(E = E_F)$$

where G_0 is the quantum of conductance.

In order to fit the parameters in the model, the experimental data were fit either to a linear or exponential trend. When fitting the experimental data, the thermopower of the **OT** series was fit to a line with a positive slope and intercept:

$$S = S_{1C} + \beta_{1S}L$$

The thermopower of the **TA** series was fit to a line with a negative slope and positive intercept:

$$S = S_{2C} - \beta_{2S}L$$

and the conductance of the **TA** series was fit to a decaying exponential:

$$G = G_{2C}\exp(-\beta_{2C}L)$$

For each series, the difference between the experimental fit and the value from the model was simultaneously minimized for all of the data available, with respect to the parameters in the model. The parameters in the model for the **OT** series were Γ, E_s, E_b, δ, and τ. The parameters for the model of the **TA** series use the parameters from the **OT** series but allow the coupling between the gateway state and the backbone, as well as the position of the gateway energy, to vary for each parameter; therefore, we minimize, with respect to E_s and τ, for each TA2 and TA3 independently and keep Γ and E_b fixed.

■ ASSOCIATED CONTENT

Supporting Information

Detailed experimental details, synthesis, and theory procedures can be found in the Supporting Information. This material is available free of charge via the Internet at http://pubs.acs.org.

■ AUTHOR INFORMATION

Corresponding Author

*E-mail: segalman@engineering.ucsb.edu.

Author Contributions

○These authors contributed equally. The manuscript was written through contributions of all authors. All authors have given approval to the final version of the manuscript.

Funding

This work is supported by the Air Force Office of Scientific Research (AFOSR) (No. MURI FA9550-12-1-0002).

Notes

The authors declare no competing financial interest.

■ ACKNOWLEDGMENTS

We thank Dr. Bhooshan Popere, Dr. Bryan MuCulloch, Prof. Shannon Yee, Prof. Fabian Pauly, and Dr. Victor Ho for their insights.

■ REFERENCES

(1) Di Ventra, M.; Pantelides, S.; Lang, N. *Phys. Rev. Lett.* **2000**, *84*, 979−982.

(2) Di Ventra, M.; Pantelides, S. T.; Lang, N. D. *Appl. Phys. Lett.* **2000**, *76*, 3448.

(3) Büttiker, M.; Imry, Y.; Landauer, R.; Pinhas, S. *Phys. Rev. B* **1985**, *31*, 6207−6215.

(4) Dell'Angela, M.; Kladnik, G.; Cossaro, A.; Verdini, A.; Kamenetska, M.; Tamblyn, I.; Quek, S. Y.; Neaton, J. B.; Cvetko, D.; Morgante, A.; Venkataraman, L. *Nano Lett.* **2010**, *10*, 2470−2474.

(5) Reed, M.; Zhou, C.; Muller, C.; Burgin, T.; Tour, J. *Science* **1997**, *278*, 252−254.

(6) Reddy, P.; Jang, S. Y.; Segalman, R. A.; Majumdar, A. *Science* **2007**, *315*, 1568−1571.

(7) Quinn, J.; Foss, F. *J. Am. Chem. Soc.* **2007**, *129*, 6714−6715.

(8) Xiao, X. Y.; Xu, B. Q.; Tao, N. J. *Nano Lett.* **2004**, *4*, 267−271.

(9) Chen, F.; Hihath, J.; Huang, Z. F.; Li, X. L.; Tao, N. J. *Annu. Rev. Phys. Chem.* **2007**, *58*, 535−564.

(10) Tao, N. J. *J. Mater. Chem.* **2005**, *15*, 3260−3263.

(11) Xu, B. Q.; Tao, N. J. J. *Science* **2003**, *301*, 1221−1223.

(12) Ahn, S.; Aradhya, S. V.; Klausen, R. S.; Capozzi, B.; Roy, X.; Steigerwald, M. L.; Nuckolls, C.; Venkataraman, L. *Phys. Chem. Chem. Phys.* **2012**, *14*, 13841−13845.

(13) Chen, W.; Widawsky, J. *J. Am. Chem. Soc.* **2011**, 17160−17163.

(14) Cheng, Z.-L.; Skouta, R.; Vazquez, H.; Widawsky, J. R.; Schneebeli, S.; Chen, W.; Hybertsen, M. S.; Breslow, R.; Venkataraman, L. *Nat. Nanotechnol.* **2011**, *6*, 353−357.

(15) Kamenetska, M.; Quek, S. Y.; Whalley, A. C.; Steigerwald, M. L.; Choi, H. J.; Louie, S. G.; Nuckolls, C.; Hybertsen, M. S.; Neaton, J. B.; Venkataraman, L. *J. Am. Chem. Soc.* **2010**, *132*, 6817−6821.
(16) Kiguchi, M.; Miura, S.; Hara, K.; Sawamura, M.; Murakoshi, K. *Appl. Phys. Lett.* **2006**, 89.
(17) Lindsay, S. *J. Chem. Educ.* **2005**, *82*, 727−733.
(18) Beebe, J.; Kim, B.; Gadzuk, J.; Frisbie, C. D.; Kushmerick, J. *Phys. Rev. Lett.* **2006**, *97*, 026801.
(19) Kiguchi, M.; Murakoshi, K. *J. Phys. Chem. C* **2008**, *112*, 8140−8143.
(20) Schneebeli, S. T.; Kamenetska, M.; Cheng, Z. L.; Skouta, R.; Friesner, R. A.; Venkataraman, L.; Breslow, R. *J. Am. Chem. Soc.* **2011**, *133*, 2136−2139.
(21) Yee, S. K.; Sun, J. B.; Darancet, P.; Tilley, T. D.; Majumdar, A.; Neaton, J. B.; Segalman, R. A. *ACS Nano* **2011**, *5*, 9256−9263.
(22) Malen, J. A.; Yee, S. K.; Majumdar, A.; Segalman, R. A. *Chem. Phys. Lett.* **2010**, *491*, 109−122.
(23) Venkataraman, L.; Park, Y. S.; Whalley, A. C.; Nuckolls, C.; Hybertsen, M. S.; Steigerwald, M. L. *Nano Lett.* **2007**, *7*, 502−506.
(24) Park, Y.; Whalley, A. *J. Am. Chem. Soc.* **2007**, *129*, 15768−15769.
(25) Capozzi, B.; Dell, E. J.; Berkelbach, T. C.; Reichman, D. R.; Venkataraman, L.; Campos, L. M. *J. Am. Chem. Soc.* **2014**, *136*, 10486−10492.
(26) Tsutsui, M.; Taniguchi, M. *Sensors (Basel)* **2012**, *12*, 7259−7298.
(27) Beebe, J. M.; Engelkes, V. B.; Miller, L. L.; Frisbie, C. D. *J. Am. Chem. Soc.* **2002**, *124*, 11268−11269.
(28) Malen, J. A.; Doak, P.; Baheti, K.; Tilley, T. D.; Segalman, R. A.; Majumdar, A. *Nano Lett.* **2009**, *9*, 1164−1169.
(29) Venkataraman, L.; Klare, J. E.; Tam, I. W.; Nuckolls, C.; Hybertsen, M. S.; Steigerwald, M. L. *Nano Lett.* **2006**, *6*, 458−462.
(30) French, W. R.; Iacovella, C. R.; Rungger, I.; Souza, A. M.; Sanvito, S.; Cummings, P. T. *J. Phys. Chem. Lett.* **2013**, *4*, 887−891.
(31) Toher, C.; Sanvito, S. *Phys. Rev. B* **2008**, *77*, 155402.
(32) Pontes, R. B.; Rocha, A. R.; Sanvito, S.; Fazzio, A.; Roque da Silva, A. J. *ACS Nano* **2011**, *5*, 795−804.
(33) Quek, S. Y.; Choi, H. J.; Louie, S. G.; Neaton, J. B. *Nano Lett.* **2009**, *9*, 3949−3953.
(34) Widawsky, J.; Chen, W.; Vázquez, H.; Kim, T.; Breslow, R.; Hybertsen, M. S.; Venkataraman, L. *Nano Lett.* **2013**, *13*, 2889−2894.
(35) Li, C.; Pobelov, I.; Wandlowski, T. *J. Am. Chem. Soc.* **2008**, *130*, 318−326.
(36) Mitsumori, T.; Inoue, K. *J. Am. Chem. Soc.* **1995**, 2467−2478.
(37) Ikeda, T.; Higuchi, M.; Sato, A.; Kurth, D. *Org. Lett.* **2008**, 2004−2007.
(38) Boer, B. De; Meng, H.; Perepichka, D.; Zheng, J.; Frank, M. M.; Chabal, Y. J.; Bao, Z. *Langmuir* **2003**, 4272−4284.